SEGMENTING CROSSING FIBER GEOMETRIES USING FLUID MECHANICS TENSOR DISTRIBUTION FUNCTION TRACTOGRAPHY

*Nathan Hageman, Alex Leow, David Shattuck, Liang Zhan, Paul Thompson, Siwei Zhu, Arthur Toga**

Laboratory of Neuroimaging
UCLA School of Medicine Department of Neurology
Los Angeles, CA

ABSTRACT

We introduce a fluid mechanics based tractography method that estimates the most likely connection path between points in a tensor distribution function (TDF) dataset. We simulated the flow of an artificial fluid whose properties are related to the underlying TDF dataset. The resulting fluid velocity was used as a metric of connection strength. We validated our algorithm using a digital phantom dataset based on a pattern with two intersecting tracts. When compared to a TDF streamline method and our single tensor fluid mechanics tractography algorithm, our method was able to segment intersecting tracts at a finer spatial resolution. Our method was successfully applied to human control data to segment a major fiber pathway, the corpus callosum, even in problematic regions with crossing fiber geometries.

***Index Terms*—** partial differential equations,fluid flow,image segmentation,magnetic resonance imaging,biomedical image processing

1. INTRODUCTION

Diffusion tensor imaging (DTI) is a magnetic resonance imaging technique used to measure the *in vivo* self-diffusion of water within tissues [1]. In the DTI reconstruction method developed by Basser *et al.*, diffusion weighted image (DWI) volumes from six or more non-collinear magnetic gradient directions are used to construct a diffusion tensor at each voxel by modeling the diffusion PDF as an anisotropic Gaussian function [1]. This diffusion tensor, D, is a symmetric 3×3 matrix that estimates the local directional dependence of anistropic diffusion. Diagonalization of the diffusion tensor yields three eigenvectors and three eigenvalues that form a basis for the set of diffusion isoprobability ellipsoids and can be used to calculate rotationally invariant scalar measures of white matter integrity [2], such as the fractional anisotropy (FA), a measure of the voxel's deviation from purely isotropic diffusion. A single tensor model is limited to resolving a single dominant fiber direction per voxel, and streamline-based tractography methods are insufficient to resolve more complex diffusion geometries, such as fiber crossings and intermixing of tracts. Although the development of surface evolution [3, 4] and partial differential equation based methods [5, 6] can more successfully approximate some of these fiber geometries, more sophisticated reconstruction models are needed to faithfully segment these kinds of architectures.

*This work was supported by the NIH through the NIH Roadmap for Medical Research, Grant U54 RR021813 entitled Center for Computational Biology (CCB). Information on the National Centers for Biomedical Computing can be obtained from http://nihroadmap.nih.gov/bioinformatics. Funding for this project was also provided by P41-RR013642 (PI: Toga)

Advances in high angular resolution (HARDI) reconstruction methods provide a means to represent more than one dominant fiber direction per voxel. Techniques, such as Q-ball imaging, reconstruct the fiber probability density functions (PDF) from the raw HARDI signal [7]. Spherical deconvolution and other deconvolution methods can express multiple fiber directions as linear combinations of a set of basis functions or higher order tensors [8, 9]. A deconvolution-like method proposed by Leow *et al.*, the tensor distribution function (TDF) framework, is a flexible model for representing multiple fiber crossings in HARDI [10]. Using the calculus of variations, the TDF approach can separate different dominant fiber directions in each voxel and compute their individual eigenvalues.

Previous work using fluid mechanics based tractography has demonstrated superior performance vs. other competing streamline and PDE-based methods in resolving crossing fiber geometries in single tensor data [6]. In this paper, we extend the fluid mechanics model to incorporate this TDF framework. We model local viscosity of the fluid and pressure forces using values derived from the TDF dataset. The incorporation of these pressure and convection terms in our flow field calculation allows us to closely couple the magnitude and direction of the fluid velocity to the underlying dominant fiber directions. To compute an estimate of the most likely connection path between two regions in the dataset, we simulate the flow of an artificial fluid between those two points through a volume whose dimensions, pressure, and local viscosity are derived from the underlying TDF data. The estimated connection path is computed by finding the optimal path through the fluid velocity vector field that maximizes a metric that is proportional to the fluid velocity and its gradient.

2. METHODS

2.1. Tensor Distribution Function Framework

In conventional single tensor reconstruction techniques, the image intensity at each voxel is related to the diffusion tensor through a Fourier transform of the displacement probability function. The tensor distribution function approach proposed by Leow *et al.* [10] extends the single tensor formulation by representing the diffusion signal at each voxel by a sum of weighted rank-2 tensors, collectively defined by a probability tensor distribution function, P(D).

The TDF approach is usually implemented by constraining all fibers to be cylindrical.

This allows each diffusion tensor to be represented by 3 values: ν, a single eigenvector corresponding to the principal direction of diffusion; λ_1, the diffusion constant in that direction; and λ_2, the diffusion constant in the plane orthgonal to ν. The TDF can then be expressed as a linear combination of these diffusion ellipsoids.

The expected value of these dominant fiber directions can be computed from the maxima of the tensor orientation distribution (TOD) function, $TOD(\nu) = \int_\lambda P(D(\lambda,\nu))\ d\lambda$, where $D(\lambda,\nu)$ is the diffusion tensor that corresponds to a particular eigenvalue, λ and direction, ν.

2.2. Fluid Model Construction

The Navier-Stokes equations describe the flow of a viscous Newtonian fluid through a pressure tensor field. In a generalized coordinate system, in the absence of external forces, and with conservation of mass, the Navier-Stokes equations simplify to

$$\frac{\partial \rho v_i}{\partial t} + \nabla \cdot (\rho v_i \overline{\mathbf{v}}) = \nabla \cdot (\mu \nabla v_i) - |(\nabla \cdot \overline{\mathbf{P}})_i|, \qquad (1)$$

where $\overline{\mathbf{v}} = \{v_i\}$ in $\mathbb{R}^3$, μ is the viscosity, ρ is the fluid density, and $\overline{\mathbf{P}}$ is the pressure tensor.

These equations provide a way of solving for the velocity field of a fluid given its pressure and viscosity. In previous work, we modeled the pressure and viscosity using scalar measures derived from a single diffusion tensor and used the fluid velocity as a metric of connection strength [6]. Here, we extend this model to the TDF framework by modeling the pressure and viscosity using the optimal TDF, $P^*(D)$.

We derive the pressure field for our model by considering the pressure tensor at each voxel as a weighted sum of the prolate diffusion tensors that correspond to the dominant fiber directions in that voxel computed from the TOD, $\overline{\mathbf{P}} = \sum_i w_i D_i(\lambda,\nu)$, where the set of $w_i D_i(\lambda,\nu)$ represent the weighted (w_i) dominant fiber directions as computed from the TOD. The local maximum pressure vectors at any position are coincident with the major computed fiber direction of the corresponding voxel. This choice has the effect of coupling the flow dynamics with the local diffusion profile.

In previous work, the local viscosity for our artificial fluid was proportional to the local fractional anisotropy. This viscous force therefore had the property of restricting fluid flow in areas of low anisotropy or coherence, such as gray matter and CSF. We chose an analogous formulation for the viscous force by using the exponential isotropy, a measure of overall anisotropy derived from the TDF function proposed by Leow *et al.*, the exponential isotropy (EI) [10]. EI is derived from the Shannon entropy $H(P(D)) = -\int_{D\in\mathbb{D}} P(D)\log(P(D))\ dD$, which measures the randomness of a probabilistic ensemble, and is formulated as $EI = e^{H(P(D))}$. Since the EI is a measure of isotropy and is high in gray matter and CSF, we model the viscous force as $\mu = \mathrm{k}(1 - \overline{EI})$, where $\overline{EI} = EI_i/EI_{max}$ is the EI for voxel, i, normalized by the maximum EI computed in the dataset. The parameter k can be adjusted to control the overall strength of the viscous force.

2.3. Numerical Solution Using the Finite Volume Method

Because an analytical solution to the Navier-Stokes equations is impossible with all but the most trivial models, we used a finite volume approach similar to our previous work to obtain an approximate numerical solution of the steady state, $\frac{\partial \rho v_i}{\partial t} = 0$. Dirichlet boundary conditions were imposed at the boundary of the brain volume, which was defined using a hand-drawn mask volume. The flux of fluid across the boundary was set to zero to prevent the loss of the artificial fluid from the brain volume, $\overline{v}(p) = 0\ \ \forall p \in \partial\Omega$, where $\overline{\mathbf{v}}(p) = \{v_i\} \in \mathbb{R}^3$ at point p, an arbitrary point on the boundary of the brain volume, $\partial\Omega$.

Each voxel was considered as a discrete control volume, V, and the Navier-Stokes momentum equations were integrated across it. The derivatives in the Navier-Stokes equations were evaluated at the faces of each control volume using a hybrid differencing scheme. Our hybrid differencing scheme assumed an upwind differencing scheme between the control volume, α, and its neighbor, β, for cells which had a Peclet (Reynolds) number (the ratio of the relative strengths of convection to diffusion) greater than 2. Otherwise, the derivatives at the control volume faces were evaluated using a central differencing scheme.

Numerical integration yielded a system of linear equations equal to the dimensions of the image volume. Because of the unique form of this large 3-D linear system, we used a variant tridiagonal matrix algorithm (TDMA) to solve for the fluid velocity vector field at the current time step [11]. We implemented the additive operator splitting (AOS) method described by Weickert *et al.*, which avoided any directional dependence in the obtained solution by eliminating the problem of multiplicative splitting [12]. This method was iteratively applied until a user-defined convergence criterion was reached. For all the experiments in this paper, we used a convergence criterion of $(V^i - V^{i-1}) < .05V^{i-1}$, where V^i was the solution to the fluid velocity vector field at time, $t = i$.

2.4. Computing Probable Connections

Once we had a solution for the fluid velocity vector field, we estimated the most likely connection path between two seed regions by finding the optimal path which maximized a weighted function of the magnitude of the fluid velocity and its gradient. Our approach was based on the generalized gradient vector flow (GGVF) method proposed by Xu *et al.* [13, 14]. The optimal path, expressed as a parameterized curve $r(s) = [x(s), y(s), z(s)]$ with $s \in [0,1]$, minimized the following energy functional, $E = \frac{1}{2}\int_0^1 [\alpha|r'(s)|^2 + \beta|r''(s)|^2] + (\Phi(r(s),t))]\ ds$.

Parameters α and β are weighting factors, determining the influence of the curve's tension or rigidity, respectively. The choice of α and β can be made based on *a priori* information about the geometry of the tract of interest. In the experiments shown in this paper, we assumed no *a priori* knowledge, and therefore we always set α and β equal to unity (1). $\Phi(r(s),t)$ is the GGVF field, $\Phi(r,t)$, restricted to the curve, r, parameterized by s, and was calculated using the same technique described by [6]

2.5. Implementation of a Streamline Tractography Method

In order to compare our method to streamline tractography approaches, we implemented a tractography method based on the Fiber Assessment by Continuous Tracking (FACT) method [15]. To generate a probable connection path between any two ROIs in the volume, a seed point was chosen within one of those ROIs, designated as the start ROI. For the single tensor datasets, we iteratively evolved the tract by starting from the seed point and moving along the major diffusion direction at the current position by a user-defined step-size until the second ROI was reached. The tract was immediately terminated and the tract rejected if the FA ever dropped below 0.4 at any point in the tract or if the diffusion direction from voxel to voxel changed by more than 60 degrees. These termination criteria were based on values proposed by Mori *et al.* [15].

For the TDF datasets, we evolved the tract from the seed region using a simulated random walk. At each step, t, the direction chosen by the evolving tract for the next step $t+1$, μ^{t+1}, was randomly chosen from the weighted dominant fiber directions, $\{w_i\nu_i^1\}$. A random

number, r, was generated from the uniform distribution [0,1]. The direction for the next step was chosen to be $\mu^{t+1} = \nu_i^1$, if the following condition was satisfied, $\sum_{n=0}^{i} w_n < r < \sum_{n=0}^{i+1} w_n$. Tracking was iteratively continued in this manner until the second ROI was reached. The tract was immediately terminated and the tract rejected if $(1 - \overline{EI})$ ever dropped below 0.4 at any point in the tract or if the diffusion direction from voxel to voxel changed by more than 60 degrees.

3. RESULTS

We applied our method to computer generated phantom data to assess its effectiveness in segmenting crossing fiber structures. We also applied our method to a human control DWI dataset to test its ability to segment major white tracts. The computational cost of this algorithm can vary widely, depending on the size of the data set and the algorithm parameters supplied by the user. We performed a timed simulation, generating 1000 probable connection paths on a control DTI dataset 192×192×55 with resolution 1.25×1.25×2.5 mm^3, 64 gradient directions with uniform spherical sampling, and b values 0 and 1000 s / mm^{-3}, on a Dell Intel 3.8 GHz dual Xeon processor workstation with 4 GB RAM. To compute the velocity vector field for the entire brain, the computational time was (330.25 minutes) 5.5 hours. To compute the probable connection paths, the computational time was (204.31 minutes) 3.4 hours.

3.1. Construction of Digital Crossing Fiber Phantom

To assess the performance of our method in resolving crossing fiber geometries, we created a digital TDF phantom using a pattern with two intersecting tracts. We modeled the ground truth as two tracts intersecting at an angle ϕ (Figure 1A). The diffusion profile of each voxel in the TDF dataset where the two tracts intersect was represented by two prolate ellipsoids with dominant diffusion directions ν_A^1 and ν_B^1 separated by the intersection angle ϕ (Figure 1B). Diffusion at these voxels was assumed to have diffusion tensor eigenvalues, $\lambda_{1,2,3}$, consistent with published values for cerebral white matter, $\lambda_{1,2,3} = \{1700, 200, 200\}$ [16], for both fiber directions. An analogous single tensor dataset was constructed for each TDF dataset according to the same underlying ground truth. The diffusion profile of each voxel in the single tensor dataset where the two tracts intersect was represented by a single oblate ellipsoid. The two fiber directions, given by ν_1 and ν_2, were represented by the eigenvalues and eigenvectors of the ellipsoid.

3.2. Comparative Validation of Fluid Mechanics Method in Segmenting Crossing Fiber Phantom

To assess the performance of our method versus a streamline based method in segmenting crossing fiber tract geometries, we generated a series of TDF and single tensor digital phantom datasets for values of ϕ ranging from 1.25 degrees to 90 degrees. For each TDF dataset, we applied both the fluid mechanics and streamline methods to a set of 1000 randomly generated seed points. We applied the fluid mechanics method to the corresponding single tensor dataset using the same set of seed points. Figure 2 shows the fraction of seed points for each method that successfully segmented the crossing tract phantom for a given value of ϕ. Our method was able to segment crossing fibers at a finer spatial resolution than the streamline approach for angles less than 60 degrees. In addition, the fluid mechanics method was more robust in segmenting crossing fiber geometries on the TDF dataset than the single tensor dataset.

3.3. Segmentation of Corpus Callosum in Human Control Data

To ascertain the ability of our method to segment major white matter tracts in the human brain, we applied our method to a human control TDF dataset to segment the corpus callosum. An individual subject was scanned on a Bruker Medspec 4 Tesla MRI scanner with a transverse electromagnetic (TEM) headcoil using a diffusion-sensitized MRI protocol. The protocol used 94 diffusion-sensitized gradient directions, and 11 baseline scans ($b = 0$) with no diffusion sensitization. Multiple seed points were randomly chosen from a mid-sagittal view of the corpus callosum on a directionally encoded color (DEC) volume. Figure 3 shows the segmentation results together with a surface model of the brain volume. Our method was able to completely reconstruct both the anterior and posterior callosal limbs. These are normally difficult regions for conventional single tensor tractography techniques because of intersecting fibers from the internal capsule. The TDF framework was able to successfully represent the crossing fibers in these voxels, and our method successfully segmented the entire corpus callosum structure.

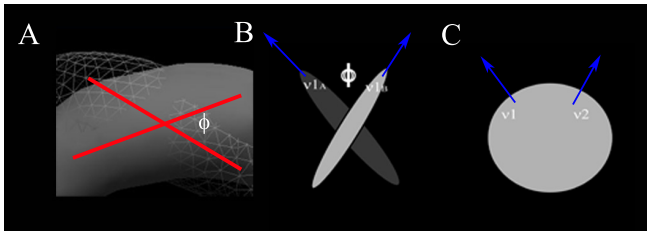

Fig. 1. Digital crossing fiber phantom constructed for comparative validation. A. Ground truth paradigm. Each dataset was generated from a ground truth of two intersecting tracts (wireframe and gray) whose tract spines (intersecting red lines) are separated by an angle, ϕ. B. For each TDF datasets, voxels in the dataset where the two tracts in A intersect are represented by two prolate ellipsoids with eigenvalues, λ_1^A and λ_1^B. C. For the single tensor datasets, voxels in the dataset where the two tracts in A intersect are represented by a single oblate ellipsoid with equal eigenvalues $\lambda_1 = \lambda_2$.

4. DISCUSSION

In this paper, we have introduced a fluid mechanics tractography method that estimates connectivity between regions in TDF datasets. Previous work has shown that fluid mechanics based approaches to single tensor DTI tractography are advantageous because they are robust to noise and can approximate complex fiber crossing geometries. Since the TDF framework can successfully represent intra-voxel crossing fibers, extension of our single tensor fluid mechanics tractography algorithm to these TDF datasets provided a robust method for accurately segmenting complex fiber geometries. We validated our technique against a competing streamline-based tractography method using a digital TDF phantom dataset based on a pattern with two intersecting tracts. Our method was able to segment the two underlying tracts with a finer spatial resolution than our streamline-based TDF method or our single tensor fluid mechanics tractography method. The phantoms are limited to a maximum of two dominant fiber directions per voxel, so it is currently unknown whether our method will continue to be superior for voxels with three of more dominant fiber directions.

Using normal human brain DWI data, we demonstrated that our algorithm can segment a major fiber pathway, the corpus callosum.

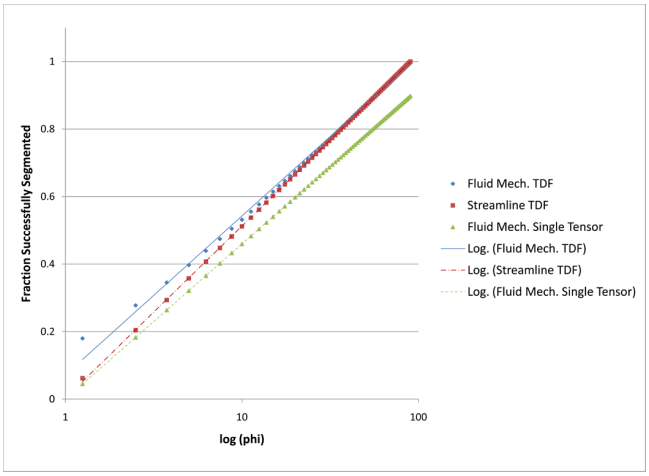

Fig. 2. Performance of fluid mechanics method vs. streamline method to segment digital crossing fiber phantom. Digital phantom datasets were constructed for a series of separation angles according to the ground truth seen in figure 1. For each dataset, a set of seed points (S = 1000) for both the fluid mechanics and streamline techniques were randomly chosen from within the dataset. Corresponding single tensor datasets were also generated for each ϕ. The graph shows the fraction of seed points that successfully segmented the two crossing tracts for various values of ϕ for (1) fluid mechanics method on the phantom TDF dataset, (2) streamline method on the phantom TDF dataset, and (3) fluid mechanics method on the single tensor dataset.

In particular, our method was able to fully reconstruct the callosal limbs - regions that are difficult for conventional tractography methods to segment because of crossing fibers of the internal capsule. Current and future work is focused on comparative validation in the human dataset using varied major fiber pathways and application to human datasets with white matter pathology.

5. REFERENCES

[1] P.J. Basser, J. Mattiello, and D. Le Bihan, "Estimation of the effective self-diffusion tensor from the NMR spin echo," *Journal of Magnetic Resonance*, vol. 103, pp. 247–254, 1994.

[2] P.J. Basser and C. Pierpaoli, "Microstructural and physiological features of tissue elucidated by quantitative diffusion tensor MRI," *Journal of Magnetic Resonance*, vol. 111, pp. 209–219, 1996.

[3] G.J.M. Parker and G.J. Barker, "Estimating distributed anatomical connectivity using fast marching methods and diffusion tensor imaging," *IEEE Transactions on Medical Imaging*, vol. 21, no. 5, pp. 505–512, 2002.

[4] P. Staempfli, T. Jaermann, G.R. Crelier, S. Kollias, A. Valavanis, and P. Boesiger, "Resolving fiber crossing using advanced fast marching tractography based on diffusion tensor imaging," *Neuroimage*, vol. 30, pp. 110–120, 2006.

[5] P.G. Batchelor, D.L.G. Hill, F. Calamante, and D. Atkinson, "Study of connectivity in the brain using the full diffusion tensor from MRI," in *IPMI 2001, LNCS 2082*, 2001, pp. 121–133.

[6] N.S. Hageman, A.W. Toga, K.L. Narr, and D.W. Shattuck, "A diffusion tensor imaging tractography algorithm based on Navier-Stokes fluid mechanics," *IEEE Transactions on Medical Imaging*, vol. 28, no. 3, pp. 348–360, 2009.

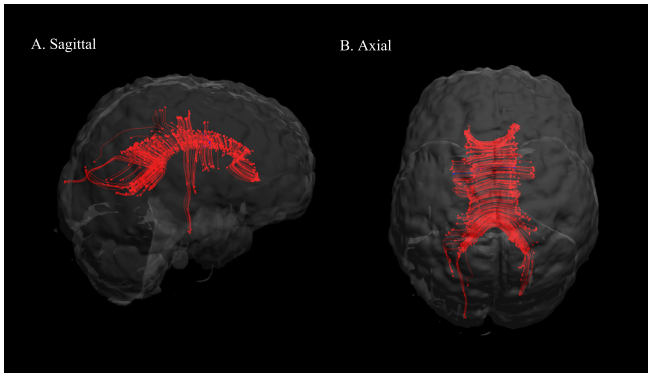

Fig. 3. Segmentation of the corpus callosum using our fluid mechanics method on TDF data from a human control subject. Seed points were chosen from a mid-sagittal view of the corpus callosum on a directionally encoded color (DEC) volume. Our method is able to completely reconstruct both the anterior and posterior callosal limbs in regions where conventional single tensor tractography techniques fail due to intersecting fibers from the internal capsule. A: Sagittal view. B: Axial view.

[7] D.S. Tuch, "Q-ball imaging," *Magnetic Resonance in Medicine*, vol. 52, pp. 1358–1372, 2004.

[8] J.D. Tournier, Fernando Calamate, David G. Gadian, and Alan Connelly, "Direct estimation of the fiber orientation density function from diffusion-weighted MRI data using spherical deconvolution," *Neuroimage*, vol. 23, pp. 1176–1185, 2004.

[9] E. Ozarslan, T. Shepherd, Baba C. Vemuri, S. Blackband, and T. Mareci, "Resolution of complex tissue microarchitecture using the diffusion orientation transform (dot)," *Neuroimage*, vol. 31, no. 3, pp. 1083–1106, 2006.

[10] A.D. Leow, S. Zhu, L. Zhan, G.I. de Zubicaray, M. Meredith, M. Wright, A.W. Toga, and P.M. Thompson, "The tensor distribution function," *Magn Reson Med*, vol. 61, no. 1, pp. 205–214, 2009.

[11] L.H. Thomas, "Elliptic problems in linear difference equations over a network," Tech. Rep., Columbia University, 1949, Watson Sci. Comput. Lab. Report.

[12] J. Weickert, B.M. ter Haar Romeny, and M.A. Viergever, "Efficient and reliable schemes for nonlinear diffusion filtering," *IEEE Transactions on Image Processing*, vol. 7, no. 3, pp. 398–410, 1998.

[13] C. Xu and J.L. Prince, "Generalized gradient vector flow external forces for active contours," *Signal Processing*, vol. 71, pp. 131–139, 1998.

[14] C. Xu and J.L. Prince, "Snakes, shapes, and gradient vector flow," *IEEE Transactions on Image Processing*, vol. 1, no. 3, pp. 359–369, March 1998.

[15] S. Mori, B.J. Crain, V.P. Chacko, and P.C.M. van Zijl, "Three dimensional tracking of axonal projections in the brain by magnetic resonance imaging," *Annals of Neurology*, vol. 45, pp. 265 – 269, 1999.

[16] C. Pierpaoli, P. Jezzard, P.J. Basser, A. Barnett, and G. Di Chiro, "Diffusion tensor MR imaging of the human brain," *Radiology*, vol. 201, no. 3, pp. 637–648, 1996.